J. Fluid Mech. (2009), *vol.* 634, *pp.* 405–418.
doi:10.1017/S0022112009990590 Printed in the United Kingdom

Feedback control by low-order modelling of the laminar flow past a bluff body

JESSIE WELLER[1], SIMONE CAMARRI[2] AND ANGELO IOLLO[1]†

[1]Institut de Mathématiques de Bordeaux, UMR CNRS 5251, Université Bordeaux 1 – INRIA MC2 project team, 33405 Talence, France

[2]Dipartimento di Ingegneria Aerospaziale, Università di Pisa, 56122 Pisa, Italy

(Received 6 March 2009 and in revised form 21 May 2009)

In this work a two-dimensional laminar flow past a square cylinder is considered. Actuators placed on the cylinder enable active control by blowing and suction. Proportional feedback control is then applied using velocity measurements taken in the cylinder wake. Projection onto an empirical subspace is combined with a calibration technique to build a low-order model of the incompressible Navier–Stokes equations. This model is used within an optimization method to determine a set of feedback gains which reduces the unsteadiness of the wake at $Re = 150$. The resulting controlled flows are further characterized by computing the critical Reynolds numbers for the onset of the vortex shedding instability.

1. Introduction

Low-order models make it possible to devise or to optimize controls for large-scale problems that would not otherwise be solvable in terms of computational size. Several such models have been successfully applied to control the wake of a circular cylinder (see, for instance, Gillies 1998; Bergmann, Cordier & Brancher 2005). In this work we investigate the possibility of applying these approaches to an actuator-based feedback control. Suboptimal controls of this kind, leading to drag reduction, have previously been devised experimentally, or using full-order models. We refer to the review paper by Choi, Jeon & Kim (2008) for examples. From a low-order modelling point of view, this problem is challenging since in general this type of model is not robust with respect to variations of the actuator control laws. This is particularly true when, like in realistic cases, the actuators and sensors are small compared to the scales of the flow.

A reduced order model (ROM) can be obtained by performing a projection of the equations of interest onto a low-dimensional subspace. In the following, this subspace is constructed empirically using velocity field data combined with the proper orthogonal decomposition (POD) technique. POD was originally introduced for the study of coherent structures (Lumley 1967) and has since been widely used in reduced-order modelling (Holmes, Lumley & Berkooz 1996). Galerkin projection of the incompressible Navier–Stokes equations onto the POD subspace leads to a model that is often incapable of correctly reproducing the data that was used to build it. Calibration techniques can however be used to identify the coefficients of the

† Email address for correspondence: angelo.iollo@math.u-bordeaux1.fr

reduced-order model such that its predictions are as close as possible to the full-order solution (Galletti *et al.* 2004). Here, we use the calibration method developed in Weller, Lombardi & Iollo (2009) for building an accurate model of an actuated flow which is fitted simultaneously to the dynamics resulting from applying a set of reference control laws. This model also gives good approximations when integrated with control laws that do not belong to the reference set, within a given trust-region.

In this paper we present a classical gradient based algorithm where the Navier–Stokes equations are replaced by the low-order system. The low-order system is updated within the optimization process by adapting the modelling techniques presented in Weller *et al.* (2009). As an example, we consider the flow past a confined square cylinder as a prototype of wake flows past bluff bodies with separation points imposed by the geometry. The control objective is to reduce the unsteadiness induced by vortex shedding. The actuation is provided by two synchronized jets driven in opposite phase, and velocity sensors are placed in the near wake. Similar configurations were studied in both experimental and numerical set-up for the case of a circular cylinder. Roussopoulos (1993) showed experimentally that for a Reynolds number 20 % over the critical limit for the onset of the two-dimensional vortex shedding (defined here Re_{cr}), the feedback of a velocity sensor could stabilize the flow using acoustic actuators on the channel sides. The feedback gain and the location of the sensor were both found empirically. In the numerical set-up of Park, Ladd & Hendricks (1994) the actuation is placed on the cylinder surface and the velocity sensor is also in the wake. By choosing the appropriate actuator gain and sensor placement it was possible to stabilize the flow for a Reynolds number of the same order as the one considered by Roussopoulos (1993).

The idea of approximating a computationally expensive problem by a low-order model to make large scale optimization problems feasible, sometimes referred to as surrogate-based optimization (Robinson *et al.* 2008), is applied in a variety of ways in the literature, each approach having relative advantages and disadvantages with respect to the one presented here. In Gerhard *et al.* (2003) a distributed actuator (a volume force) and a localized sensor were used to devise a feedback control to stabilize the vortex shedding past a circular cylinder at a Reynolds number twice Re_{cr}. An observer was employed to estimate the state of the flow and the control law was inferred using the POD model. The feedback control resulted in reduction of the flow unsteadiness. The same configuration was studied more recently in King *et al.* (2008) where a pre-computed control law was updated in real time as a function of the estimated state of the system (model predictive control). This approach was more effective (a less unsteady flow) than the one developed in Gerhard *et al.* (2003), based more on physical insight. Samimy *et al.* (2007) implemented a feedback control derived by a classical linear-quadratic approach to stabilize an experimental cavity flow. The linearized POD model was obtained by particle image velocimetry data relative to forced and unforced experiments. Combining these data, different reduced models were obtained. A significant reduction of the resonant tone was reported in some cases, depending on the POD model employed. Other approaches are those based on vortex models as done for a circular cylinder at a Reynolds number 50 % above Re_{cr} in Protas (2004). The control and the observer were built starting from a point vortex model and actuation was performed by cylinder rotation leading to an effective reduction of the wake oscillation was obtained. In Pastoor *et al.* (2008) an experimental feedback shear layer control for bluff body drag reduction was proposed. The two jets actuating the flow were driven by a controller designed using a vortex method, and the control resulted in drag reduction.

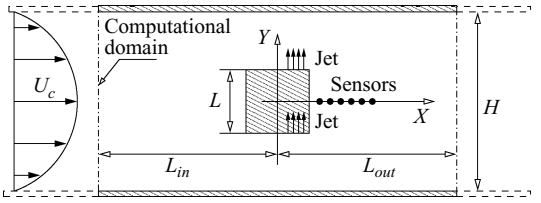

FIGURE 1. Flow configuration and computational domain.

In this work we focus on a strategy for wake stabilization that employs localized actuators and sensors in order to be as realistic as possible. The state of the flow is not estimated, and hence we need not design an observer. The gain coefficients between the sensors and the actuators are the parameters to be optimized using a nonlinear low-order model. In the spirit of what was done experimentally in Samimy *et al.* (2007), the low-order model incorporates in a systematic way the dynamics of the controlled flows that are obtained during the optimization process. The overall approach can be extended in principle to more complex three-dimensional flows. The Reynolds number considered is close to the limit for the onset of three-dimensional wake instabilities and is more than twice Re_{cr}. In addition, the separation points are fixed by the geometry independently of the actuation. This case represents a challenging configuration to apply the proposed low-order model based optimization method.

2. A reduced-order model for actuated flow

2.1. *Flow and control set-up*

We consider a two-dimensional laminar flow past a confined square cylinder. A sketch showing the geometry, the frame of reference and the adopted notation is plotted in figure 1.

The incoming flow is assumed to have a Poiseuille profile, while non-reflecting characteristic based boundary conditions are imposed at the outlet. No-slip conditions are enforced both on the cylinder and on the parallel walls. With reference to figure 1, $L/H = 1/8$, $L_{in}/L = 12$, $L_{out}/L = 20$. Details concerning the grids and the numerical set-up are reported in Buffoni *et al.* (2006). In the following the Reynolds number is defined with respect to the cylinder side and the maximum value of the inlet velocity profile.

In this flow configuration the computational domain is well defined and the boundary conditions are simple and easily reproduced in an eventual experiment. A Von Kármán vortex street develops past the cylinder when the Reynolds number increases above $Re_{cr} = 59$ as a result of a global instability (Camarri & Giannetti 2007). The Reynolds number we considered in this work is $Re = 150$. The resulting flow is two-dimensional and it is characterized by clearly developed vortices. The flow can indeed be safely considered two-dimensional up to a Reynolds number of 160 (Camarri & Giannetti 2007).

Two actuators are placed on the cylinder and are driven in opposite phase, as shown in figure 1:

$$v(\boldsymbol{x}, t) = c(t).$$

The centre of the jets are placed close to the rear separation point at $x/L = 0.3$ and $y/L = -0.5$ and $y/L = 0.5$, respectively, and their width is $0.16L$. Driving them in

opposite phase allows the use of only one control law, making modelling as simple as possible while simulating a reasonable experimental set-up. The velocity profile of the actuators is constant across the jet and the numerical implementation of the actuators is similar to what is done for inlet and outlet boundary conditions.

Actuation is started when the flow is fully developed. The sensors are placed in the cylinder wake providing centreline transverse velocity measurements. A feedback control law is then defined by

$$c(t) = \sum_{j=1}^{N_s} \mathsf{K}_j v(\boldsymbol{x}_j, t), \tag{2.1}$$

where v denotes the transverse component of the velocity, N_s the number of sensors and K_j the gains applied to each measurement.

2.2. *Reduced-order modelling by POD and calibration*

Empirical modelling is an approach for reducing the size of large scale nonlinear systems when full-dimensional control is not possible. These methods make use of numerical or experimental data to retrieve ROM that are less accurate than the original models but far less expensive to solve. These models suffer from being largely dependant on the set of solutions that was used to build them. It is therefore important to include a wide range of dynamics in the database. In our case this meant considering a sufficiently long time period and an appropriate set of different control laws. Therefore, we choose a time period, denoted $[0, T]$, that includes about six shedding cycles (sampled with 30 snapshots per cycle), and a set of control laws to be specified later:

$$\mathscr{C} = \{c^1, \ldots, c^{N_c}\} \quad c^\ell \in \mathscr{C}^1([0, T]) \quad \ell = 1 \ldots N_c,$$

The instantaneous velocity at time t^i, resulting from applying a control c^ℓ is denoted $\boldsymbol{u}^{i,\ell}$. A snapshot database, depending on the control set $\mathscr{C}$, and denoted $\mathscr{S}(\mathscr{C})$, is then defined as

$$\mathscr{S}(\mathscr{C}) = \{\boldsymbol{u}^{i,\ell}(\boldsymbol{x})\}_{i=1\ldots N_t, \ell=1\ldots N_c}.$$

POD is used to obtain a low-dimensional subspace of $P = span\{\mathscr{S}(\mathscr{C})\}$. Given a solution subspace P, of size N, POD consists in determining a set of N_r orthogonal functions $\{\boldsymbol{\Psi}^r\}$, with $N_r \leqslant N$, such that the error, resulting from projecting an element of P onto $span\{\boldsymbol{\Psi}^r\}$ is minimal.

In this work, a modified database was formed to lift the boundary conditions:

$$\mathscr{S}_0(\mathscr{C}) = \{\boldsymbol{w}^{i,\ell}(\boldsymbol{x}) = \boldsymbol{u}^{i,\ell}(\boldsymbol{x}) - \boldsymbol{u}_0(\boldsymbol{x}) - \boldsymbol{u}_c(\boldsymbol{x}) c^\ell(t^i)\}_{i=1\ldots N_t, \ell=1\ldots N_c},$$

where $\boldsymbol{u}_0$ and $\boldsymbol{u}_c$ are velocity fields chosen to ensure $\boldsymbol{w}^{i,\ell}$ is equal to zero on all boundaries. They are chosen as in Galletti *et al.* (2007). Two simulations are performed with constant control laws which we denote c^ν and c^μ, with $c^\nu = 0$ and $c^\mu \neq 0$. The fields $\boldsymbol{u}_0$ and $\boldsymbol{u}_c$ are then defined by

$$\boldsymbol{u}_0(\boldsymbol{x}) = \frac{1}{N_t} \sum_{i=1}^{N_t} \boldsymbol{u}^{i,\nu}(\boldsymbol{x}) \text{ and } \boldsymbol{u}_c(\boldsymbol{x}) = \frac{1}{c^\mu} \left(\frac{1}{N_t} \sum_{i=1}^{N_t} \boldsymbol{u}^{i,\mu}(\boldsymbol{x}) - \boldsymbol{u}_0(\boldsymbol{x}) \right).$$

Any choice of c^μ results in the velocity field $\boldsymbol{u}_c$ being equal to 1 on the control boundary while the rest of the field depends on the value of this constant. So as not to create important perturbations near the cylinder, c^μ was chosen to be relatively small ($c^\mu = -0.05$). The main concern is to lift the solution with a sufficiently

regular function to avoid pathological situations such as discontinuities. By taking a physically reasonable function we avoid the introduction of source terms that may lead to ill-conditioned problems in the identification process.

Denoting $\boldsymbol{\Phi}^r(\boldsymbol{x})$ the spatial modes resulting from applying POD to $\mathscr{S}_0(\mathscr{C})$, a reduced-order solution denoted $\boldsymbol{u}_R$ is defined by

$$\boldsymbol{u}_R(\boldsymbol{x}, t) = \boldsymbol{u}_0(\boldsymbol{x}) + c(t)\boldsymbol{u}_c(\boldsymbol{x}) + \sum_{r=1}^{N_r} a_r(t)\boldsymbol{\Phi}^r(\boldsymbol{x}), \tag{2.2}$$

where the $a_r(t)$ are scalar functions of time.

Performing a Galerkin projection of the incompressible Navier–Stokes equations onto the N_r-dimensional subspace spanned by the POD modes, yields a system of ODEs:

$$\begin{aligned} \dot{a}_r(t) &= \boldsymbol{f}(\boldsymbol{a}(t), c(t), \dot{c}(t)) \cdot \boldsymbol{X}_r, \\ a_r(0) &= (\boldsymbol{u}(\cdot, 0) - \boldsymbol{u}_0 - c(0)\boldsymbol{u}_c, \boldsymbol{\Phi}^r), \qquad \text{for } 1 \leqslant r \leqslant N_r, \end{aligned} \tag{2.3}$$

where $\boldsymbol{X}_r$ is a $M_r = N_r^2 + 2N_r + 4$ element vector:

$$\boldsymbol{X}_r = \left[A_r, \{B_{rk}\}_{k=1,N_r}, \{C_{rks}\}_{k,s=1,N_r}, E_r, F_r, G_r, \{H_{rk}\}_{k=1,N_r}\right]^t,$$

with, for $1 \leqslant r, k, s \leqslant N_r$:

$$\begin{aligned} A_r &= -((\boldsymbol{u}_0 \cdot \nabla)\boldsymbol{u}_0, \boldsymbol{\Phi}^r) + \frac{1}{Re}(\Delta \boldsymbol{u}_0, \boldsymbol{\Phi}^r), \\ B_{rk} &= -((\boldsymbol{u}_0 \cdot \nabla)\boldsymbol{\Phi}^k, \boldsymbol{\Phi}^r) - ((\boldsymbol{\Phi}^k \cdot \nabla)\boldsymbol{u}_0, \boldsymbol{\Phi}^r) + \frac{1}{Re}(\Delta \boldsymbol{\Phi}^k, \boldsymbol{\Phi}^r), \\ C_{rks} &= -((\boldsymbol{\Phi}^k \cdot \nabla)\boldsymbol{\Phi}^s, \boldsymbol{\Phi}^r), \\ E_r &= -(\boldsymbol{u}_c, \boldsymbol{\Phi}^r), \\ F_r &= -(\boldsymbol{u}_c \cdot \nabla \boldsymbol{u}_0, \boldsymbol{\Phi}^r), \\ G_r &= -((\boldsymbol{u}_0 \cdot \nabla)\boldsymbol{u}_c, \boldsymbol{\Phi}^r) - ((\boldsymbol{u}_c \cdot \nabla)\boldsymbol{u}_0, \boldsymbol{\Phi}^r) + \frac{1}{Re}(\Delta \boldsymbol{u}_c, \boldsymbol{\Phi}^r), \\ H_r &= -((\boldsymbol{u}_c \cdot \nabla)\boldsymbol{\Phi}^k, \boldsymbol{\Phi}^r) - ((\boldsymbol{\Phi}^k \cdot \nabla)\boldsymbol{u}_c, \boldsymbol{\Phi}^r), \end{aligned}$$

and $\boldsymbol{f}(\boldsymbol{a}(t), c(t), \dot{c}(t))$ is a vector function defined by

$$\boldsymbol{f}(t) = \left[1, \{a_k(t)\}_{k=1,N_r}, \{a_k(t)a_s(t)\}_{k,s=1,N_r}, \dot{c}(t), c^2(t), c(t), \{a_k(t)c(t)\}_{k=1,N_r}\right].$$

Model accuracy can be evaluated by integrating (2.3) with one of the control laws in $\mathscr{C}$, and comparing the solution $\boldsymbol{a}(t)$ with the projection coefficients of the Navier–Stokes solution $\boldsymbol{u}$ onto the low-order subspace spanned by the POD modes. Denoting $\hat{a}_k(t) = (\boldsymbol{u}(\cdot, t) - \boldsymbol{u}_0 - c(t)\boldsymbol{u}_c, \boldsymbol{\Phi}^k)$, we define the ROM integration error by:

$$\sum_{r=1}^{N_r} \int_0^T (\hat{a}_r(t) - a_r(t))^2 \, \mathrm{d}t.$$

In some cases, system (2.3), with coefficients $\boldsymbol{X}_r$ determined by Galerkin projection, turns out to be unstable, and in most other cases the integration error defined above is relatively large. However, efficient calibration techniques can be applied to build a similarly structured model (Galletti *et al.* 2004, 2007; Couplet, Basdevant & Sagaut 2005). A computationally inexpensive approach consists in seeking $\boldsymbol{X}_r$ such that the residual, resulting from injecting the temporal projection coefficients $\hat{\boldsymbol{a}}(t)$ into the equations (2.3), is minimized. Such a residual can be calculated for each control law

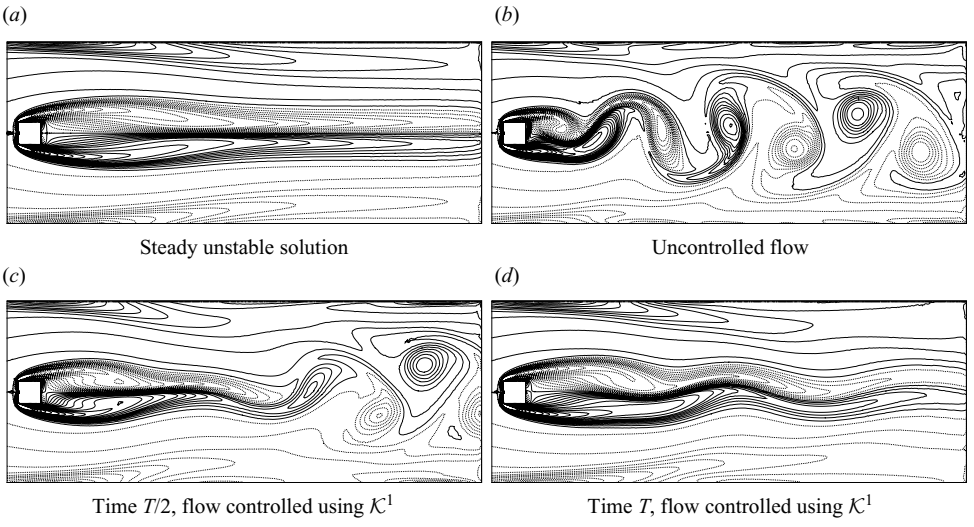

FIGURE 2. Vorticity of the flow downstream of the cylinder. Isolines are the same in all figures.

in $\mathscr{C}$. The calibration problem is then formulated

$$\min_{\boldsymbol{X}_r} \sum_{r=1}^{N_r} \sum_{\ell=1}^{N_c} \int_0^T \left(\dot{\hat{a}}_r^\ell(t) - \boldsymbol{f}(\hat{\boldsymbol{a}}^\ell(t), c^\ell(t), \dot{c}^\ell(t)) \cdot \boldsymbol{X}_r \right)^2 \mathrm{d}t \tag{2.4}$$

In fact, only a subset of $\boldsymbol{X}_r$ is identified. For the tensor C_{rks} we keep the values obtained from the Galerkin projection in order to improve the conditioning of the linear problem resulting from calibration. This method is investigated in Weller *et al.* (2009), where it is shown that if $N_c = 1$ the model is accurate when integrated with the control that was used to generate the database but not robust to a variation of the control law. Moreover, in that paper it is also shown that increasing N_c from 1 to 2 or 3 greatly improves the ROM robustness to a variation of the control law.

3. A ROM-based algorithm for optimization

The aim is to exploit the reduced order model to damp vortex shedding in the cylinder wake. To this end, we choose to minimize the difference between the actuated flow velocity and the steady unstable solution $\bar{\boldsymbol{u}}$ (see figure 2*a*), as done in Li & Aubry (2003), over a fixed period of time $[0, T]$. Minimizing this cost functional also enables drag reduction, yet does not require any knowledge of the pressure field. Furthermore the centreline transverse velocity of the objective velocity field $\bar{\boldsymbol{u}}$ is zero, meaning that if the flow is actuated by using a feedback based on this quantity, the velocity of the jets tends to zero as the flow is stabilized.

The functional to minimize is defined by

$$J(\boldsymbol{u}) = \int_0^T F(\boldsymbol{u}(t))\,\mathrm{d}t, \tag{3.1}$$

where F denotes the difference in norm at each time:

$$F(\boldsymbol{u}(t)) = \|\boldsymbol{u}(\cdot, t) - \bar{\boldsymbol{u}}\|_2^2.$$

Reduced-order models have been applied previously with some success for solving optimization problems. In these works, a classic optimization procedure was applied to minimize the cost functional, using the ROM to calculate the descent directions at each step. Within the optimization loop, the model was periodically updated using a trust region principle (Bergmann & Cordier 2008). Each update corresponded to a new numerical simulation of the Navier–Stokes equations, and therefore a new database, and an evaluation of the actual value of the functional. We use a similar approach in this work.

A difficulty in the present application is that the ROM can give a good approximation of a solution, while the model-based gradient fails to be a descent direction for the original infinite-dimensional problem. The ROM-based optimization algorithms can therefore reach sets of control parameters that cause an increase in the functional. This is due to the fact that ROMs are very sensitive to parameter variation. The multi-dynamic ROM defined in the previous paragraph leads to models that are more robust. However, including large sets of data in the POD–ROM procedure can be costly, and also implies a loss of accuracy. Indeed the residuals of the mean square problem (defined in (2.4)) increase as we include additional control laws in the calibration processes, that is as we add constraints to the minimization problem. This implies that the POD model becomes less accurate for the controlled flows belonging to the database. The idea of our optimization algorithm is to use N_c-control models, with N_c as small as possible, and to increase N_c if the current model supplies a wrong direction.

We first define the projected functional. Using (2.2) and (3.1), $J(\boldsymbol{u}_R)$ can be expanded as a function of a and c, which we denote $J_R(\boldsymbol{a}, c)$:

$$J_R(\boldsymbol{a}, c) = \|\boldsymbol{u}_0 - \bar{\boldsymbol{u}}\|^2 + c^2(t)\|\boldsymbol{u}_c\|^2 + 2c(t)(\boldsymbol{u}_0 - \bar{\boldsymbol{u}}, \boldsymbol{u}_c) + \sum_{k=1}^{N_r} \left(2a_k(t)(\boldsymbol{u}_0 - \bar{\boldsymbol{u}}, \boldsymbol{\Phi}^k) + 2a_k(t)c(t)(\boldsymbol{u}_c, \boldsymbol{\Phi}^k) + a_k^2(t)\right).$$

The initial control law is denoted c^0. A full-order simulation is performed over $[0, T]$ using this control. POD is then applied to the snapshot database $\mathscr{S}_0(\{c^0\})$ and a 1-control model, denoted $R^0(\boldsymbol{a}, c)$, is built using the method described previously. A descent method is then applied to solve the following problem:

$$\min_c J_R(\boldsymbol{a}, c) \quad \text{s. t.} \quad R^0(\boldsymbol{a}, c). \tag{3.2}$$

We estimate the model is only reliable for control laws that do not differ too much from c^0. This trust-region is defined at the beginning of the optimization procedure, and is not modified. The descent is therefore stopped as soon as the relative variation of the control law, measured using the L^2 norm on $[0, T]$, reaches $\Delta = 40\,\%$. This limit was found by a trial and error procedure as a compromise between computational cost and accuracy of the gradient. If Δ is small, the gradient obtained by using the low-order model is likely to be more accurate with respect to a case where Δ is large. However, this implies that the number of optimization steps performed without updating the low-order model by additional Navier–Stokes simulations is smaller, which in turn means that the computational costs are higher. Once a suboptimal control c^{new} is reached, a new full-order simulation is performed, and the new value of the cost functional is evaluated. POD is applied to $\mathscr{S}_0(\{c^0, c^1\})$ and and a 2-control model $R^1(\boldsymbol{a}, c)$ is built using this data. The procedure is repeated using

$R^1(\boldsymbol{a}, c)$, descent starts from c^{new} if the functional has indeed decreased, and from c^0 otherwise.

Continuing this way we defined an optimization algorithm in which the ROM is updated at the end of each step, and the current suboptimal control law is updated only if a better one is found. The optimization algorithm structure is the following:

(i) Initialise : $k=0$, $\mathscr{C}^0=\{c^0\}$
Perform full-order simulation using c^0. Solution is denoted $\boldsymbol{u}^0$
Set $c^{opt}=c^0$ and $J^{opt}=J(\boldsymbol{u}^0)$
(ii) Apply POD to $\mathscr{S}_0(\mathscr{C}^k)$ to obtain a low-dimensional subspace
(iii) Build calibrated model $R^k(\boldsymbol{a}, c)$
(iv) Begin descent method to solve:

$$c^{new} = arg \min_c J_R(\boldsymbol{a}, c) \text{ s.t. } R^k(\boldsymbol{a}, c)$$

$$\text{while } \int_0^T (c^{opt}-c^{new})^2 \,\mathrm{d}t < \Delta^2 \int_0^T (c^{opt})^2 \,\mathrm{d}t \qquad \text{(model trust-region)}$$

(v) Evaluate $J^{new}=J(\boldsymbol{u}^{new})$ (perform full order simulation using c^{new}.)
(a) If $J^{new} < J^{opt}$: Choice of c^{new} is validated.
$\mathscr{C}^{k+1}=\{c^{opt}, c^{new}\}$
$c^{opt} \leftarrow c^{new}$ and $J^{opt} \leftarrow J^{new}$
(b) If $J^{new} > J^{opt}$: choice of c^{new} rejected.
$\mathscr{C}^{k+1}=\mathscr{C}^k \cup \{c^{new}\}$
c^{opt} and J^{opt} unchanged
(vi) $k \leftarrow k+1$, go to (ii).

The above loop is interrupted if the decrease rate of J reaches a certain threshold or if a multi-dynamic model providing a correct descent direction cannot be found. Although the convergence of the algorithm towards the solution of the full-order optimization problem is not guaranteed, the test on the actual value of the functional at each iteration prevents divergence. Using the ROM at step (iv) makes the algorithm much more efficient computationally than an algorithm using the full order model: the gradient calculation involved in finding a descent direction is simple to implement and calculated in negligible time. In the present set-up the control law $c(t)$ is optimized in the space of the gains $\mathscr{K}=\{\mathsf{K}_1, \ldots, \mathsf{K}_{N_s}\}$, in agreement with (2.1). At each optimization step the control $c(t)$ is changed by updating $\mathscr{K}$.

4. Results and discussion

The proportional feedback control (defined in (2.1)) was used with $N_s=16$ sensors. At the first optimization step, the initial guess for the gain coefficients was $\mathsf{K}_3=-1$ and $\mathsf{K}_j=0$ for $j \neq 3$. The sensors were uniformly distributed on the symmetry line in the near wake between $x/L=0.75$ and $x/L=2.625$. The vorticity field resulting from the application of the suboptimal gain coefficients obtained after 17 iterations of the above algorithm is plotted in figure 2. At the 18th iteration, the model did not provide a descent direction and was therefore updated as described in the previous section. However, the new model also failed, as did the next. The procedure was therefore interrupted although the gradient obtained with the ROM was still not negligible at this step. An explanation for this is that as the functional reaches its minimum, the decrease that can be achieved at each iteration is lower than the model error. Figure 3(a) shows the time evolution of $F(\boldsymbol{u}(t))$ at different stages in the optimization. We note that at each optimization step there is an instant in the

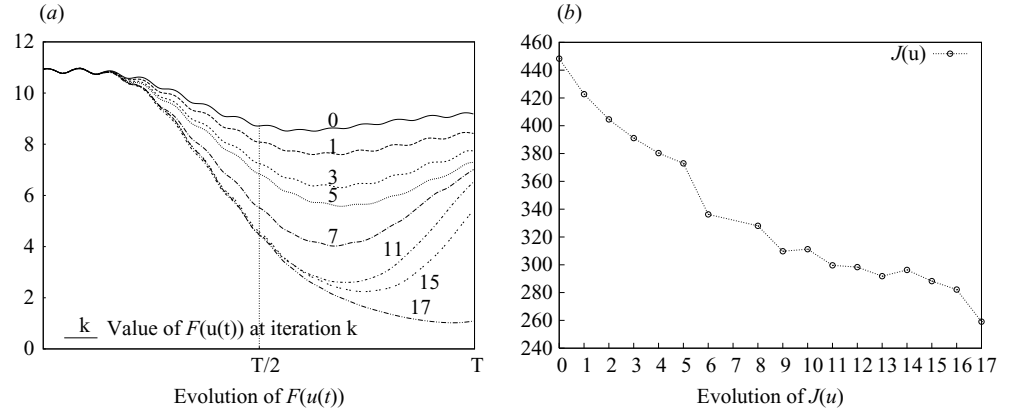

FIGURE 3. Evolution of the functionals $F(\boldsymbol{u}(t))$ and $J(\boldsymbol{u})$.

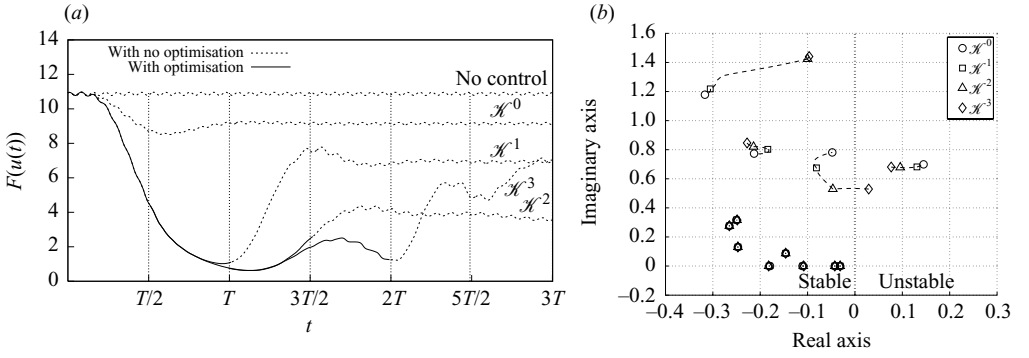

FIGURE 4. (*a*): Time evolution of the functional $F(\boldsymbol{u}(t))$ versus time and (*b*) eigenvalues of the linearized Navier–Stokes at $Re = 150$ for the uncontrolled and controlled cases.

$[0, T]$ time interval at which $F(\boldsymbol{u}(t))$ is minimal. The more $J(\boldsymbol{u})$ decreases (as the optimization proceeds), the more this point nears T. At iteration 17, it is almost at the end of the time interval. In figure 3(*a*) it is seen that the evolution of $F(\boldsymbol{u}(t))$ forms an envelope as the optimization proceeds. The time interval over which the solution remains unchanged increases with the iteration number and hence the minimum of the curve is progressively moved to the right. This suggests that the last control reached by the algorithm is nearly optimal. Evolution of the cost functional $J(\boldsymbol{u})$ is depicted in figure 3(*b*). Two controls were rejected during the procedure. This is visible in figure 3(*b*): $J(\boldsymbol{u})$ increases twice, at steps 10 and 14. The total decrease during optimization is of 42 %.

The optimization performed provided a suboptimal control law for the time interval $[0, T]$, but the simulation was continued outside this interval up to time $3T$ using the same set of sensors and gains. Let us define $\mathscr{K}^0$ the set of gains corresponding to the initial optimization guess and $\mathscr{K}^1$ the set corresponding to the gains obtained from optimizing on $[0, T]$. The control laws corresponding to $\mathscr{K}^0$ and $\mathscr{K}^1$ are plotted in figure 5(*a*), where it is seen that the actuation decreases as the flow unsteadiness is reduced. We note that the control laws are remarkably different even though $\mathscr{K}^0$ corresponds to a feedback with only one sensor for which the dominant gain is very close to that of $\mathscr{K}^1$. Figure 4(*a*) shows the time evolution of $F(\boldsymbol{u}(t))$ during the period

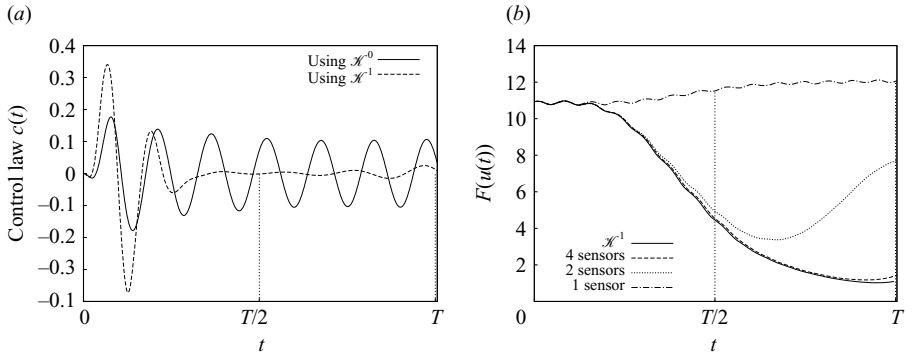

FIGURE 5. Effects of applying $\mathscr{K}^1$.

$[0, 3T]$ obtained with $\mathscr{K}^0$ and $\mathscr{K}^1$. It can be seen that beyond T the solution obtained using $\mathscr{K}^1$ develops large scale oscillations that are however asymptotically less intense than those corresponding to both the uncontrolled system and $\mathscr{K}^0$. Accordingly, the asymptotic mean drag coefficient decreases from 1.409 in the uncontrolled case to 1.316 in the case relative to $\mathscr{K}^1$. Comparing $\mathscr{K}^0$ and $\mathscr{K}^1$ it can be seen that small differences in the gain values induce large variations in the controlled system behaviour over the optimization time interval. In figure 5(b) we show the effect of applying the gain coefficients of $\mathscr{K}^1$ redistributed over a smaller number of sensors. For example, we placed 4 sensors at $x/L = 1$, $x/L = 1.5$, $x/L = 2$ and $x/L = 2.5$, and associated to each point a gain obtained by adding up the gains associated to the surrounding sensors. The effect on $F(\boldsymbol{u}(t))$ was almost identical to that obtained using all 16 sensors. However, while this means that 16 sensors were not necessary to obtain the actuator signal, when the 4 sensors are lumped to 2 ($x/L = 1.25$, $x/L = 2.25$) or to 1 ($x/L = 1.75$), the control effect is radically modified.

In order to improve the stabilization beyond T a new optimization was performed over the time interval $[T/2, 3T/2]$, starting from the initial conditions corresponding to the actual state of the controlled flow at time $T/2$. The initial guess for the gains was equal to $\mathscr{K}^1$ and the algorithm performed 9 loops before exiting. The new set of gain coefficients obtained after optimization is denoted $\mathscr{K}^2$. Evolution of $F(\boldsymbol{u}(t))$ over $[T/2, 3T/2]$ when the gains $\mathscr{K}^2$ are applied starting from time $T/2$ (feedback coefficients $\mathscr{K}^1$ are applied in the interval $[0, T/2]$) is shown in figure 4(a). Using $\mathscr{K}^2$ instead of $\mathscr{K}^1$ over $[T/2, T]$, induces only a small decrease in $F(\boldsymbol{u}(t))$, whereas a substantial reduction can be observed over $[T, 3T/2]$. Outside the optimization interval the asymptotic solution is less unsteady than the solution obtained with gains $\mathscr{K}^0$ and $\mathscr{K}^1$, and the asymptotic mean drag coefficient is equal to 1.283. Following the same principle, a third optimization was performed over $[T, 2T]$ with similar results: a minimal reduction of $F(\boldsymbol{u}(t))$ over $[T, 3T/2]$, but a substantial improvement over $[3T/2, 2T]$. When the gains corresponding to the last optimization performed (denoted $\mathscr{K}^3$) are applied beyond $2T$, the flow rapidly develops an additional instability as it seen in figure 4(a). The feedback gains corresponding to the four controls are reported in table 1.

Since the functional is defined on a finite time horizon, the control may well tend to achieve the best performance on that interval regardless of what will happen outside. The solution outside this interval is not considered in the control and in this sense is not predictable. The main difficulty here is that the problem is nonlinear and hence

x/L	0.75	0.875	1	1.125	1.25	1.375	1.5	1.625
$\mathscr{K}^0$	0	0	−1	0	0	0	0	0
$\mathscr{K}^1$	−0.0098	−0.0088	−1.0076	−0.0037	0.0028	0.0118	0.0241	0.0372
$\mathscr{K}^2$	−0.2785	−0.2485	−1.2355	−0.233	−0.2331	−0.2295	−0.2158	−0.1854
$\mathscr{K}^3$	−0.2455	−0.2118	−1.1965	−0.1911	−0.1884	−0.1818	−0.1641	−0.1293
x/L	1.75	1.875	2	2.125	2.25	2.375	2.5	2.625
$\mathscr{K}^0$	0	0	0	0	0	0	0	0
$\mathscr{K}^1$	0.0505	0.059	0.0713	0.0834	0.0916	0.1035	0.1165	0.1314
$\mathscr{K}^2$	−0.1385	−0.0931	−0.0052	0.1121	0.209	0.3797	0.5844	0.8197
$\mathscr{K}^3$	−0.0772	−0.0279	0.0666	0.1914	0.2934	0.4734	0.6877	0.9327

TABLE 1. Values of feedback gains for the three optimization procedures. The sensors are identified by their position x/L.

we do not have tools such as the Riccati equation to ensure asymptotic stability of the controlled system.

For a further characterization of the three sets of feedback coefficients described above, the corresponding critical Reynolds number for the onset of the primary instability of the wake was evaluated by a linear stability analysis. To this purpose, the two-dimensional incompressible Navier–Stokes equations were discretized in space by a second-order centred finite-difference scheme on a two-dimensional Cartesian staggered grid. The body was represented by an immersed-boundary technique. A Newton method was used to find the steady solution of the equations and a Krylov subspace method was used to compute some eigenvalues of the equations linearized about the steady solution. After a first localization of the eigenvalues, a shift-invert spectral transformation was used for their final localization in the complex plane. The same numerical ingredients described in Giannetti & Luchini (2007) ware used here, and they were already validated for the same flow configuration without actuators in Camarri & Giannetti (2007).

After having carried out a grid convergence study using five progressively refined grids with the computational domain of figure 1, the final results were obtained on a non-uniform grid with 810 and 494 points in the x and y directions, respectively, having 135 uniformly distributed nodes on each cylinder side and about 22 points on each jet orifice. Using this grid we found that Re_{cr} for the three set of feedback coefficients $\mathscr{K}^1$, $\mathscr{K}^2$ and $\mathscr{K}^3$ is approximately equal to 79, 107 and 115, respectively, whereas for the uncontrolled case $Re_{cr} = 59$. Following the above results, two full Navier–Stokes simulations were carried out for each set of feedback coefficients, one in the stable regime and one in the unstable. All the simulations were started from a fully developed vortex-shedding regime and the feedback control was impulsively applied at a given time. For the simulation, the same code used for building the low-order models was adopted. As a result, the feedback coefficients $\mathscr{K}^1$, $\mathscr{K}^2$, $\mathscr{K}^3$ drove the flow towards the steady target solution, thus stabilizing the flow completely, at Reynolds numbers equal to 75, 100 and 110, respectively. Conversely, the unsteadiness of the vortex shedding was not eliminated at Reynolds numbers equal to 85, 110 and 120, respectively. For a case of complete stabilization ($Re = 110$ and control $\mathscr{K}^3$), the aerodynamic coefficients are plotted in figure 6.

Finally, a linear stability analysis at $Re = 150$ was carried out for each of the three sets of feedback coefficients. In particular, the 13 most unstable eigenvalues were localized in the complex plane. In this linear analysis the amplification factor

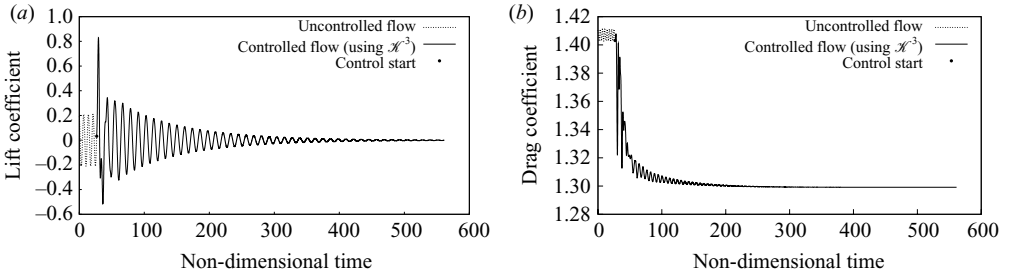

FIGURE 6. Effect of $\mathscr{K}^3$ at $Re = 110$. The beginning of each plot shows lift and drag for the fully developed uncontrolled flow.

is the real part of the eigenvalues, which is thus positive for unstable eigenmodes (exponential growth). In figure 4(*b*) we plot the eigenvalues (only one for each complex–conjugate couple) for the uncontrolled case and for the three sets of feedback coefficients. In order to identify the eigenvalues that are displaced by the control, the trajectory of each eigenvalue is plotted (dashed line) considering a continuous linear transition between the uncontrolled case, $\mathscr{K}^1$, $\mathscr{K}^2$ and $\mathscr{K}^3$ in this order. The fact that another couple of eigenvalues cross the imaginary axes when passing from control $\mathscr{K}^2$ to control $\mathscr{K}^3$ can explain the behaviour of the controlled flow beyond $2T$. Nevertheless, passing from control $\mathscr{K}^1$ to $\mathscr{K}^3$, Re_{cr} is systematically increased. As a final remark concerning these results, we stress that there is no guarantee that a full stabilization is possible at $Re = 150$ with this control set-up. Indeed it has been proved that complete stabilization of the incompressible Navier–Stokes equations via wall-actuation is possible when using full-state feedback (Raymond 2006), but as we use a limited number of sensors, and therefore have a limited knowledge of the state, this property no longer holds.

5. Conclusions

We considered the problem of applying an optimization method based on a low-order model to the minimization of the flow unsteadiness in a bluff body wake. We showed that it is possible to make use of reduced-order modelling to determine a suboptimal solution to this problem, at least on a limited time interval. Although our approach does not guarantee a particular behaviour of the flow outside this interval, it was found that the feedback chosen this way leads to a long term reduction in drag. A stability analysis indicated that the eigenvalues corresponding to linearly unstable modes are shifted toward the stable region of the complex plane. However, a previously stable eigenvalue was perturbed in such a way as to move to the unstable region (control $\mathscr{K}^3$) thus increasing the unsteadiness outside the optimization time interval. Nonetheless, the critical Reynolds number is systematically increased as the optimization time interval is shifted. The computed controls are able to stabilize the flow starting from the saturated instability at Reynolds numbers close to the linear stability limit for the corresponding control. In particular, it was possible to obtain a complete stabilization of the wake at a Reynolds number that is almost the double of the stability limit for the considered configuration.

The control strategy as well as many other parameters of the approach described were not optimized. For example, the placement of actuators and sensors has not been carried out based on systematic arguments, the control target could have been improved using a different cost functional, another overlapping of the optimization

time intervals could have led to better results, opting for an adaptive trust region algorithm would probably accelerate the convergence of the optimization method, to list just a few possibilities. Nevertheless, the results show that the procedures is sufficiently robust to actually perform an effective optimization within the selected time horizon. In perspective, the objective is to investigate more complex control strategies, control objectives other than stabilization, more realistic flow configurations.

The authors are grateful to Alain Dervieux and Bruno Koobus for making the AERO code available for the Navier–Stokes simulations, Flavio Giannetti and Paolo Luchini for making available the computational tools for the linear stability analysis. The support of IDRIS and M3PEC for CPU time, and of the ANR COBORD are kindly acknowledged.

REFERENCES

Bergmann, M. & Cordier, L. 2008 Optimal control of the cylinder wake in the laminar regime by trust-region methods and POD reduced-order models. *J. Comput. Phys.* **227** (16), 7813–7840.

Bergmann, M., Cordier, L. & Brancher, J.-P. 2005 Optimal rotary control of the cylinder wake using POD reduced order model. *Phys. Fluids* **17** (9), 097101.

Buffoni, M., Camarri, S., Iollo, A. & Salvetti, M. V. 2006 Low-dimensional modelling of a confined three-dimensional wake flow. *J. Fluid Mech.* **569**, 141–150.

Camarri, S. & Giannetti, F. 2007 On the inversion of the Kármán street in the wake of a confined square cylinder. *J. Fluid Mech.* **574**, 169–178.

Choi, H., Jeon, W.-P. & Kim, J. 2008 Control of flow over a bluff body. *Annu. Rev. Fluid Mech.* **40**, 113–139.

Couplet, M., Basdevant, C. & Sagaut, P. 2005 Calibrated reduced-order POD-Galerkin system for fluid flow modelling. *J. Comput. Phys.* **207** (1), 192–220.

Galletti, B., Bottaro, A., Bruneau, C.-H. & Iollo, A. 2007 Accurate model reduction of transient and forced wakes. *Eur. J. Mech.* B/*Fluids* **26**, 354–366.

Galletti, B., Bruneau, C. H., Zannetti, L. & Iollo, A. 2004 Low-order modelling of laminar flow regimes past a confined square cylinder. *J. Fluid Mech.* **503**, 161–170.

Gerhard, J., Pastoor, M., King, R., Noack, B. R., Dillmann, A., Morzyński, M. & Tadmor, G. 2003 Model-based control of vortex shedding using low-dimensional Galerkin models. In *Thirty-third AIAA Fluids Conference and Exhibit*. Paper 2003–4262, Orlando, FL, USA.

Giannetti, F. & Luchini, P. 2007 Structural sensitivity of the first instability of the cylinder wake. *J. Fluid Mech.* **581**, 167–197.

Gillies, E. A. 1998 Low-dimensional control of the circular cylinder wake. *J. Fluid Mech.* **371**, 157–178.

Holmes, P., Lumley, J. L. & Berkooz, G. 1998 *Turbulence, Coherent Structures, Dynamical Systems and Symmetry*. Cambridge University Press.

King, R., Aleksic, K., Gelbert, G., Losse, N., Muminovic, R., Brunn, A., Nitsche, W., Bothien, M., Moeck, J., Paschereit, C., Noack, B., Rist, U. & Zengl, M. 2008 Model predictive flow control – invited paper. In *Thirty-eight AIAA Fluid Dynamics Conference and Exhibit*. Paper 2008–3975, Seattle, Washington, U.S.A.

Li, F. & Aubry, N. 2003 Feedback control of a flow past a cylinder via transverse motion. *Phys. Fluids* **15**, 2163–76.

Lumley, J. L. 1967 The structure of inhomogeneous turbulent flows. In *Atmospheric Turbulence and Radio Wave Propagation* (ed. A. M. Yaglom & V. L. Tatarski), pp. 166–178. Nauka.

Park, D. S., Ladd, D. M. & Hendricks, E. W. 1994 Feedback control of von Kármán vortex shedding behind a circular cylinder at low Reynolds numbers. *Phys. Fluids* **6**, 2390–2405.

Pastoor, M., Henning, L., Noack, B. R., King, R. & Tadmor, G. 2008 Feedback shear layer control for bluff body drag reduction. *J. Fluid Mech.* **608**, 161–196.

Protas, B. 2004 Linear feedback stabilization of laminar vortex shedding based on a point vortex model. *Phys. Fluids* **16**, 4473–4488.

Raymond, J.-P. 2006 Boundary feedback stabilization of the two dimensional Navier–Stokes equations. *SIAM J. Control Optim.* **45**(3), 790–828.

Robinson, T., Eldred, M., Willcox, K. & Haimes, R. 2008 Surrogate-based optimization using multifidelity models with variable parameterization and corrected space mapping. *AIAA J.* **46** (11), 2814–2822.

Roussopoulos, K. 1993 Feedback control of vortex shedding at low Reynolds numbers. *J. Fluid Mech.* **248**, 267–296.

Samimy, M., Debiasi, M., Caraballo, E., Serrani, A., Yuan, X., Little, J. & Myatt, J. H. 2007 Feedback control of subsonic cavity flows using reduced-order models. *J. Fluid Mech.* **579**, 315–346.

Weller, J., Lombardi, E. & Iollo, A. 2009 Robust model identification of actuated vortex wakes. *Physica* D **238**, 416–427.